First Double-Differential Measurement of Kinematic Imbalance in Neutrino Interactions with the MicroBooNE Detector

P. Abratenko,[35] O. Alterkait,[35] D. Andrade Aldana,[15] J. Anthony,[5] L. Arellano,[20] J. Asaadi,[34] A. Ashkenazi,[32] S. Balasubramanian,[12] B. Baller,[12] G. Barr,[25] J. Barrow,[21,32] V. Basque,[12] O. Benevides Rodrigues,[15,31] S. Berkman,[12] A. Bhanderi,[20] M. Bhattacharya,[12] M. Bishai,[3] A. Blake,[17] B. Bogart,[22] T. Bolton,[16] J. Y. Book,[14] L. Camilleri,[10] D. Caratelli,[4] I. Caro Terrazas,[9] F. Cavanna,[12] G. Cerati,[12] Y. Chen,[28] E. O. Cohen,[32] J. M. Conrad,[21] M. Convery,[28] L. Cooper-Troendle,[39] J. I. Crespo-Anadón,[6] M. Del Tutto,[12] S. R. Dennis,[5] P. Detje,[5] A. Devitt,[17] R. Diurba,[2] Z. Djurcic,[1] R. Dorrill,[15] K. Duffy,[25] S. Dytman,[26] B. Eberly,[30] A. Ereditato,[2] J. J. Evans,[20] R. Fine,[18] O. G. Finnerud,[20] W. Foreman,[15] B. T. Fleming,[39] N. Foppiani,[14] D. Franco,[39] A. P. Furmanski,[23] D. Garcia-Gamez,[13] S. Gardiner,[12] G. Ge,[10] S. Gollapinni,[33,18] O. Goodwin,[20] E. Gramellini,[12] P. Green,[20,25] H. Greenlee,[12] W. Gu,[3] R. Guenette,[20] P. Guzowski,[20] L. Hagaman,[39] O. Hen,[21] R. Hicks,[18] C. Hilgenberg,[23] G. A. Horton-Smith,[16] B. Irwin,[23] R. Itay,[28] C. James,[12] X. Ji,[3] L. Jiang,[37] J. H. Jo,[3,39] R. A. Johnson,[8] Y.-J. Jwa,[10] D. Kalra,[10] N. Kamp,[21] G. Karagiorgi,[10] W. Ketchum,[12] M. Kirby,[12] T. Kobilarcik,[12] I. Kreslo,[2] M. B. Leibovitch,[4] I. Lepetic,[27] J.-Y. Li,[11] K. Li,[39] Y. Li,[3] K. Lin,[27] B. R. Littlejohn,[15] W. C. Louis,[18] X. Luo,[4] C. Mariani,[37] D. Marsden,[20] J. Marshall,[38] N. Martinez,[16] D. A. Martinez Caicedo,[29] K. Mason,[35] A. Mastbaum,[27] N. McConkey,[20,36] V. Meddage,[16] K. Miller,[7] J. Mills,[35] A. Mogan,[9] T. Mohayai,[12] M. Mooney,[9] A. F. Moor,[5] C. D. Moore,[12] L. Mora Lepin,[20] J. Mousseau,[22] S. Mulleriababu,[2] D. Naples,[26] A. Navrer-Agasson,[20] N. Nayak,[3] M. Nebot-Guinot,[11] J. Nowak,[17] N. Oza,[10,18] O. Palamara,[12] N. Pallat,[23] V. Paolone,[26] A. Papadopoulou,[1,21] V. Papavassiliou,[24] H. B. Parkinson,[11] S. F. Pate,[24] N. Patel,[17] Z. Pavlovic,[12] E. Piasetzky,[32] I. D. Ponce-Pinto,[39] I. Pophale,[17] S. Prince,[14] X. Qian,[3] J. L. Raaf,[12] V. Radeka,[3] A. Rafique,[1] M. Reggiani-Guzzo,[20] L. Ren,[24] L. Rochester,[28] J. Rodriguez Rondon,[29] M. Rosenberg,[35] M. Ross-Lonergan,[18] C. Rudolf von Rohr,[2] G. Scanavini,[39] D. W. Schmitz,[7] A. Schukraft,[12] W. Seligman,[10] M. H. Shaevitz,[10] R. Sharankova,[12] J. Shi,[5] E. L. Snider,[12] M. Soderberg,[31] S. Söldner-Rembold,[20] J. Spitz,[22] M. Stancari,[12] J. St. John,[12] T. Strauss,[12] S. Sword-Fehlberg,[24] A. M. Szelc,[11] W. Tang,[33] N. Taniuchi,[5] K. Terao,[28] C. Thorpe,[17] D. Torbunov,[3] D. Totani,[4] M. Toups,[12] Y.-T. Tsai,[28] J. Tyler,[16] M. A. Uchida,[5] T. Usher,[28] B. Viren,[3] M. Weber,[2] H. Wei,[19] A. J. White,[39] Z. Williams,[34] S. Wolbers,[12] T. Wongjirad,[35] M. Wospakrik,[12] K. Wresilo,[5] N. Wright,[21] W. Wu,[12] E. Yandel,[4] T. Yang,[12] L. E. Yates,[12] H. W. Yu,[3] G. P. Zeller,[12] J. Zennamo,[12] and C. Zhang[3]

(The MicroBooNE Collaboration)[*]

[1]*Argonne National Laboratory (ANL), Lemont, Illinois 60439, USA*
[2]*Universität Bern, Bern CH-3012, Switzerland*
[3]*Brookhaven National Laboratory (BNL), Upton, New York 11973, USA*
[4]*University of California, Santa Barbara, California 93106, USA*
[5]*University of Cambridge, Cambridge CB3 0HE, United Kingdom*
[6]*Centro de Investigaciones Energéticas, Medioambientales y Tecnológicas (CIEMAT), Madrid E-28040, Spain*
[7]*University of Chicago, Chicago, Illinois 60637, USA*
[8]*University of Cincinnati, Cincinnati, Ohio 45221, USA*
[9]*Colorado State University, Fort Collins, Colorado 80523, USA*
[10]*Columbia University, New York, New York 10027, USA*
[11]*University of Edinburgh, Edinburgh EH9 3FD, United Kingdom*
[12]*Fermi National Accelerator Laboratory (FNAL), Batavia, Illinois 60510, USA*
[13]*Universidad de Granada, Granada E-18071, Spain*
[14]*Harvard University, Cambridge, Massachusetts 02138, USA*
[15]*Illinois Institute of Technology (IIT), Chicago, Illinois 60616, USA*
[16]*Kansas State University (KSU), Manhattan, Kansas 66506, USA*
[17]*Lancaster University, Lancaster LA1 4YW, United Kingdom*
[18]*Los Alamos National Laboratory (LANL), Los Alamos, New Mexico 87545, USA*
[19]*Louisiana State University, Baton Rouge, Louisiana 70803, USA*
[20]*The University of Manchester, Manchester M13 9PL, United Kingdom*
[21]*Massachusetts Institute of Technology (MIT), Cambridge, Massachusetts 02139, USA*
[22]*University of Michigan, Ann Arbor, Michigan 48109, USA*
[23]*University of Minnesota, Minneapolis, Minnesota 55455, USA*

[24] *New Mexico State University (NMSU), Las Cruces, New Mexico 88003, USA*
[25] *University of Oxford, Oxford OX1 3RH, United Kingdom*
[26] *University of Pittsburgh, Pittsburgh, Pennsylvania 15260, USA*
[27] *Rutgers University, Piscataway, New Jersey 08854, USA*
[28] *SLAC National Accelerator Laboratory, Menlo Park, California 94025, USA*
[29] *South Dakota School of Mines and Technology (SDSMT), Rapid City, South Dakota 57701, USA*
[30] *University of Southern Maine, Portland, Maine 04104, USA*
[31] *Syracuse University, Syracuse, New York 13244, USA*
[32] *Tel Aviv University, Tel Aviv, Israel, 69978*
[33] *University of Tennessee, Knoxville, Tennessee 37996, USA*
[34] *University of Texas, Arlington, Texas 76019, USA*
[35] *Tufts University, Medford, Massachusetts 02155, USA*
[36] *University College London, London WC1E 6BT, United Kingdom*
[37] *Center for Neutrino Physics, Virginia Tech, Blacksburg, Virginia 24061, USA*
[38] *University of Warwick, Coventry CV4 7AL, United Kingdom*
[39] *Wright Laboratory, Department of Physics, Yale University, New Haven, Connecticut 06520, USA*

(Received 11 January 2023; revised 9 May 2023; accepted 14 July 2023; published 6 September 2023)

We report the first measurement of flux-integrated double-differential quasielasticlike neutrino-argon cross sections, which have been made using the Booster Neutrino Beam and the MicroBooNE detector at Fermi National Accelerator Laboratory. The data are presented as a function of kinematic imbalance variables which are sensitive to nuclear ground-state distributions and hadronic reinteraction processes. We find that the measured cross sections in different phase-space regions are sensitive to different nuclear effects. Therefore, they enable the impact of specific nuclear effects on the neutrino-nucleus interaction to be isolated more completely than was possible using previous single-differential cross section measurements. Our results provide precision data to help test and improve neutrino-nucleus interaction models. They further support ongoing neutrino-oscillation studies by establishing phase-space regions where precise reaction modeling has already been achieved.

DOI: 10.1103/PhysRevLett.131.101802

Neutrino-oscillation measurements aim to extract neutrino mixing angles, mass differences, and the charge-parity violating phase, and to search for new physics beyond the standard model [1–3]. The analysis of such measurements traditionally relies on detailed comparisons of measured and theoretically expected neutrino interaction rates in the corresponding detectors. Therefore, a precise understanding of neutrino-nucleus interactions is required to fully exploit the discovery potential of current and next-generation experiments.

With a growing number of neutrino-oscillation experiments employing liquid argon time projection chamber (LArTPC) neutrino detectors [4–9], high-accuracy modeling of neutrino-argon interactions is becoming of paramount importance [10–12]. The overarching goal of these efforts is both to achieve few-percent-level modeling of neutrino-argon interaction rates and to provide a detailed understanding of the final-state kinematics of emitted particles that are used to reconstruct the energies of the interacting neutrinos [13,14].

This Letter reports the first measurement of flux-integrated double-differential cross sections for muon-neutrino-argon (ν_μ-Ar) charged-current (CC) quasielastic (QE)-like scattering reactions as a function of transverse kinematic imbalance variables. Building upon a previous analysis of neutrino-argon cross sections with a similar signal event topology [15], we focus on reactions where the neutrino removes a single intact proton from the nucleus without producing any additional detected particles. The results reported here are obtained using the Booster Neutrino Beam (BNB) and the MicroBooNE detector at Fermi National Accelerator Laboratory with an exposure of 6.79×10^{20} protons on target.

Transverse kinematic imbalance variables were previously shown to be sensitive to the modeling of the nuclear ground-state distribution and to nuclear medium effects, such as hadronic final-state interactions (FSI) [16–21]. By measuring the components of the muon and proton momenta perpendicular to the neutrino direction, $\vec{p}_T^{\,\mu}$ and $\vec{p}_T^{\,p}$ respectively, we construct the transverse missing momentum, $\delta\vec{p}_T = \vec{p}_T^{\,\mu} + \vec{p}_T^{\,p}$, and its angular orientation with respect to $\vec{p}_T^{\,\mu}$, $\delta\alpha_T = \arccos\left[(-\vec{p}_T^{\,\mu} \cdot \delta\vec{p}_T)/(p_T^\mu\, \delta p_T)\right]$. Owing to the isotropic nature of Fermi motion, $\delta\alpha_T$ is expected to be uniformly distributed in the absence of any FSI. In the presence of FSI, the proton momentum is generally reduced and the $\delta\alpha_T$ distribution becomes enhanced toward 180°. Similarly, the shape of the δp_T distribution encapsulates information related to Fermi motion and is further smeared due to FSI and multinucleon effects. Given the sensitivity of $\delta\alpha_T$ to FSI and of δp_T to both FSI and Fermi motion, a simultaneous measurement of these two observables can help to disentangle the individual impact of each nuclear effect on the neutrino-nucleus interaction. Similarly, the muon-proton momentum imbalance components transverse and parallel to the transverse lepton momentum, $\delta p_{T,x} = \delta p_T \sin\delta\alpha_T$ and $\delta p_{T,y} = \delta p_T \cos\delta\alpha_T$, provide further handles on Fermi motion and FSI processes, respectively.

The active volume of the MicroBooNE LArTPC contains 85 tonnes of argon [22]. It is exposed to the BNB neutrino energy spectrum that peaks around 0.8 GeV and extends to about 2 GeV.

Neutrinos are detected by measuring the charged particles produced following their interactions with argon nuclei in the LArTPC active volume. These charged particles travel through the liquid argon, producing both scintillation light and trails of ionization electrons. In the presence of a uniform 273 V/cm electric field, the ionization electrons drift through the argon and are detected by a system of three anode wire planes that are perpendicular to the field. The scintillation light is measured by photomultiplier tubes (PMTs). Events are recorded if the PMT signals are in time coincidence with the beam arrival time. Trigger hardware and software selection cuts reject background events, mostly from cosmic muons, providing enriched data samples in which a neutrino interaction occurs in ≈15% of selected beam spills [23].

The PANDORA reconstruction package [24] is used to form individual tracks from the measured ionization signals in the enriched data samples. Particle identification and momentum determination are performed using the measured track energy-deposition profile and track length [25,26].

Candidate muon-proton pairs are identified by requiring exactly two tracklike objects and no showerlike objects based on a track-score variable from PANDORA [27,28]. The discriminant described in Ref. [29] is used to distinguish muon and proton candidates. We further apply quality cuts to avoid misreconstructed tracks. Details are given in Ref. [30].

To reduce contributions from cosmic tracks and to minimize bin-migration effects, the event selection considers only muon and proton track pairs that are fully contained within a fiducial volume of 10 cm from the edge of the detector active volume.

The signal definition used in this analysis includes all ν_μ-Ar scattering events with a final-state muon with momentum $0.1 < p_\mu < 1.2$ GeV/c and exactly one final-state proton with $0.3 < p_p < 1$ GeV/c. Events with final-state neutral pions at any momentum are excluded. Signal events may contain additional protons with momentum less than 300 MeV/c or greater than 1 GeV/c, neutrons at any momentum, and charged pions with momentum lower than 70 MeV/c. We refer to the signal events as CC1p0π. Owing to the requirement for a single proton and no pions in the final state, the CC1p0π topology of interest is dominated by QE events. Yet, more complex interactions, namely meson exchange currents (MEC), resonance interactions (RES), and deep inelastic scattering events (DIS), can still produce the CC1p0π experimental signature. Events that do not satisfy the CC1p0π signal definition at a truth level are treated as background. Such events are referred to as non-CC1p0π and are dominated by interactions with two protons in the momentum range of interest, where the second proton was not reconstructed. This topology is studied in Ref. [31], where a good data-simulation agreement is observed.

After the application of the event selection, we retain 9051 data events that satisfy all criteria. Event distributions for all the aforementioned variables of interest and details on the CC1p0π event selection, along with the corresponding systematic uncertainties, can be found in the Supplemental Material [32] and in Ref. [30].

The flux-averaged differential event rate as a function of a given variable x in bin i is obtained by

$$\frac{dR}{dx_i} = \frac{N_i - B_i}{T \cdot \Phi_\nu \cdot \Delta_i} \tag{1}$$

where N_i and B_i are the number of measured events and the expected background events, respectively. T is the number of target argon nuclei in the fiducial volume of interest. Φ_ν corresponds to the total BNB flux and, finally, Δ_i corresponds to the ith bin width or area for the single- and double-differential results, respectively.

We report the extracted cross sections for the measured interaction using the Wiener singular value decomposition (Wiener-SVD) unfolding technique as a function of unfolded kinematic variables [34]. More details on the unfolding procedure can be found in Ref. [30]. The unfolding machinery returns the unfolded differential cross section and the corresponding uncertainties. Apart from the unfolded result, an additional smearing matrix A_C is obtained, which accounts for the regularization and bias of the measurement. When a comparison to the unfolded data is performed, the corresponding A_C matrices must be applied to the true cross section predictions. See the Supplemental Material [32] for the data release, the unfolded covariance matrices, and the additional matrices A_C.

As in previous MicroBooNE measurements [15,35–37], the full Monte Carlo (MC) simulation used in the unfolding procedure consists of a combination of simulated neutrino interactions overlaid on beam-off background events. This

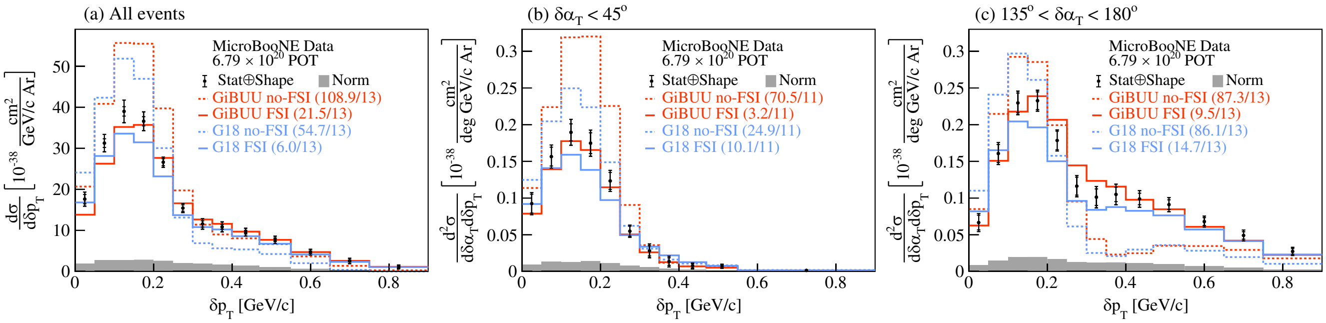

FIG. 1. The flux-integrated (a) single- and (b),(c) double- (in $\delta\alpha_T$ bins) differential CC1p0π cross sections as a function of the transverse missing momentum δp_T. Inner and outer error bars show the statistical and total (statistical and shape systematic) uncertainty at the 1σ, or 68%, confidence level. The gray band shows the separate normalization systematic uncertainty. Colored lines show the results of theoretical cross section calculations with (solid line) and without (dashed line) FSI based on the GENIE (blue) and GIBUU (orange) event generators.

provides an accurate description of the dominant cosmic backgrounds pertinent to surface detectors using real data. Neutrino interactions are simulated using the GENIE v3.0.6 event generator [38,39]. The CC QE and CC MEC neutrino interaction models have been tuned to T2K ν_μ-^{12}C CC0π data [40,41]. Predictions for more complex interactions, such as resonances, remain unaltered. No additional MC constraints are applied. We refer to the corresponding prediction as G18. The latter configuration is used to simulate both the CC1p0π signal and non-CC1p0π background events. GENIE generates all final-state particles associated with the primary neutrino interaction and propagates them through the nucleus, accounting for FSI. The particle propagation outside the nucleus is simulated using GEANT4 [42], with the MicroBooNE detector response modeled using the LArSoft framework [43,44]. Based on this simulation, we estimate that our efficiency for selecting fully contained CC1p0π events is ≈10%, with a purity of ≈70%.

The total covariance matrix $E = E^{\rm stat} + E^{\rm syst}$ used in the Wiener-SVD filter includes the statistical and systematic uncertainties associated with our measurement. $E^{\rm stat}$ is a diagonal covariance matrix including the statistical uncertainties, and $E^{\rm syst}$ is a covariance matrix incorporating the total systematic uncertainties. More details on the sources of systematic uncertainty and the construction of these matrices can be found in Ref. [30]. These matrices include uncertainties on the integrated cross section due to the neutrino flux prediction (7.3%) [45], neutrino interaction cross section modeling (6%) [38,39,41], detector response modeling (4.9%) [46], beam exposure (2.3%), statistics (1.5%), number of scattering targets (1.15%), reinteractions (1%) [47], and out-of-cryostat interaction modeling (0.2%). The full fractional uncertainty on the integrated total cross section sums to 11%.

Across the results reported in this Letter, statistical uncertainties are shown by the inner error bars on the final results. The systematic uncertainties were decomposed into shape- and normalization-related sources following the procedure outlined in Ref. [48]. The cross-term uncertainties were incorporated in the normalization part. The outer error bars on the reported cross sections correspond to statistical and shape uncertainties added in quadrature. The normalization uncertainties are presented with the gray band at the bottom of our results.

The single- and double-differential results as a function of δp_T are presented in Fig. 1. They are compared with G18 and the theory-driven GIBUU 2021 (GIBUU) event generator. Additional comparisons to the corresponding event generators when FSI are turned off are also included (G18 no-FSI and GIBUU no-FSI). G18 uses the local Fermi gas (LFG) model of the nuclear ground state [49] and the Nieves CCQE scattering prescription [50] with Coulomb corrections for the outgoing muon [51] and random phase approximation (RPA) corrections [52]. It also uses the Nieves MEC model [53], the KLN-BS resonance (RES) [54–57], and Berger-Sehgal coherent (COH) [58] scattering models. Furthermore, the hA2018 FSI model [59] and the MicroBooNE-specific tuning of model parameters [41] are utilized. GIBUU uses somewhat similar models, but, unlike GENIE, they are implemented in a coherent way by solving the Boltzmann-Uehling-Uhlenbeck transport equation [60]. The simulation includes the LFG model [49], a standard CCQE expression [61], an empirical MEC model and a dedicated spin-dependent resonance amplitude calculation following the MAID analysis [60]. The DIS model is from PYTHIA [62]. The FSI treatment is different as the hadrons propagate through the residual nucleus in a nuclear potential which is consistent with the initial state.

The single-differential results as a function of δp_T using all the events that satisfy our selection are shown in Fig. 1(a). The χ^2/bins data comparison for each generator shown on all the results takes into account the total covariance matrix, including the off diagonal elements. Theoretical uncertainties on the models themselves are not

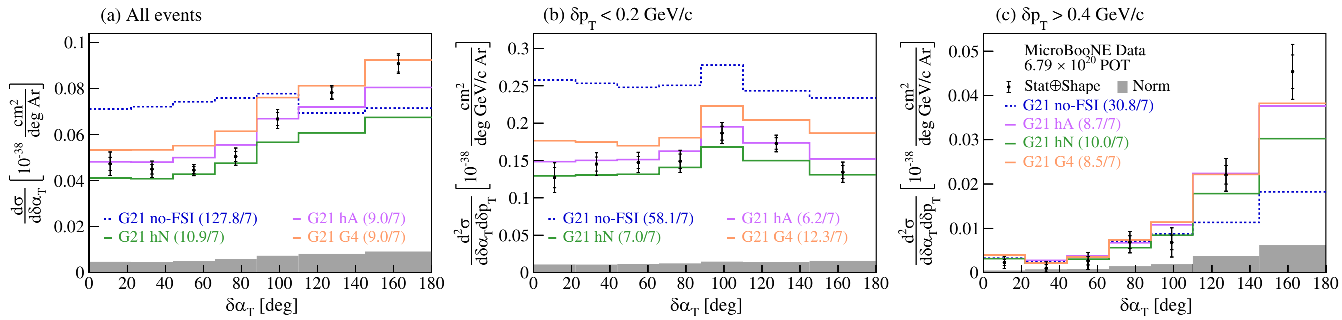

FIG. 2. The flux-integrated (a) single- and (b),(c) double- (in δp_T bins) differential CC1p0π cross sections as a function of the angle $\delta\alpha_T$. Inner and outer error bars show the statistical and total (statistical and shape systematic) uncertainty at the 1σ, or 68%, confidence level. The gray band shows the separate normalization systematic uncertainty. Colored lines show the results of theoretical cross section calculations with a number of FSI-modeling choices based on the GENIE event generator.

included. The peak height of both generator predictions is ≈30% higher when FSI effects are turned off. Yet, all distributions illustrate a transverse missing momentum tail that extends beyond the Fermi momentum (≈250 MeV/c) whether FSI effects are incorporated or not. The double-differential result using events with $\delta\alpha_T < 45°$ shown in Fig. 1(b) is dominated by events that primarily occupy the region up to the Fermi momentum and do not exhibit a high-momentum tail. The double-differential results using events with $135° < \delta\alpha_T < 180°$ are shown in Fig. 1(c) and illustrate high transverse missing momentum up to 1 GeV/c. The prediction without FSI effects is strongly disfavored. The region around 0.3 GeV/c in Fig. 1(c) shows a noticeable difference between the G18 and GIBUU predictions. This behavior could be driven by the different approaches of simulating the MEC and FSI effects between the two event generators, as can be seen in the interaction breakdown of the relevant cross sections in the Supplemental Material [32]. Therefore, the high δp_T region is an appealing candidate for neutrino experiments to benchmark and tune the FSI modeling in event generators. The same single- and double-differential cross section comparisons as a function of δp_T using different FSI variations are included in the Supplemental Material [32].

Extracted cross sections as a function of $\delta\alpha_T$ are shown in Fig. 2. Here we perform comparisons to the recently added theory-driven GENIE v3.0.6 G21_11b_00_000 configuration (G21 hN) [63]. This configuration uses the SuSAv2 model for CCQE and CCMEC interactions [64], and the hN2018 FSI model [65]. The modeling choices for RES, DIS, and COH interactions are the same as for G18. We investigated the effect of the FSI-modeling choice by comparing the G21 hN results to the ones obtained with G21 hA, where the hA2018 FSI model was used instead, and to G21 G4 with the recently coupled GEANT4 FSI framework [66]. The prediction where the FSI effects have been turned off (G21 no-FSI) is also included for comparison. The impact of different QE modeling options as a function of the same variables is investigated in the Supplemental Material [32].

The single-differential results as a function of $\delta\alpha_T$ using all the events that satisfy our selection are shown in Fig. 2(a). The prediction without FSI shows a uniform behavior as a function of $\delta\alpha_T$ and is disfavored by the data. The addition of FSI effects leads to a ≈30% asymmetry around $\delta\alpha_T = 90°$. The three FSI models used here for comparison yield a consistent behavior. The double-differential result shown in Fig. 2(b) using events with $\delta p_T < 0.2$ GeV/c illustrates a uniform distribution indicative of the suppressed FSI impact in that part of the phase space. The G21 no-FSI prediction is higher than the other FSI predictions. The difference comes from the generation of multiple particles above detection threshold due to reinteraction effects in the FSI-rich samples. Such events do not satisfy the signal definition and therefore introduce the difference in the absolute scale. The double-differential results using events with $\delta p_T > 0.4$ GeV/c are shown in Fig. 2(c) and illustrate the presence of strong FSI effects with a significantly enhanced asymmetry around 90°. Thus, the high $\delta\alpha_T$ region is highly informative for the FSI-modeling performance in event generators. See the Supplemental Material [32] for details on the interaction breakdown of the aforementioned results and Ref. [30] for further double-differential results.

Finally, Fig. 3 shows the single- and double-differential results as a function of $\delta p_{T,x}$. The result shows the comparison between the nominal G18 model using the LFG and predictions using the same G18 interaction modeling but different nuclear ground-state model options available in the GENIE event generator, namely the Bodek-Ritchie Fermi Gas (RFG) [67] and an effective spectral function (EffSF) [68]. Furthermore, the prediction without RPA effects is shown for comparison (no-RPA) [52]. The FSI impact on the same results is investigated in the Supplemental Material [32].

The single-differential result [Fig. 3(a)] illustrates a fairly broad symmetric distribution centered around 0 GeV/c. The double-differential result for events where $\delta p_{T,y} < -0.15$ GeV/c [Fig. 3(b)] illustrates an even broader distribution, as can be seen in the widths (σ_{Data}) of Gaussian

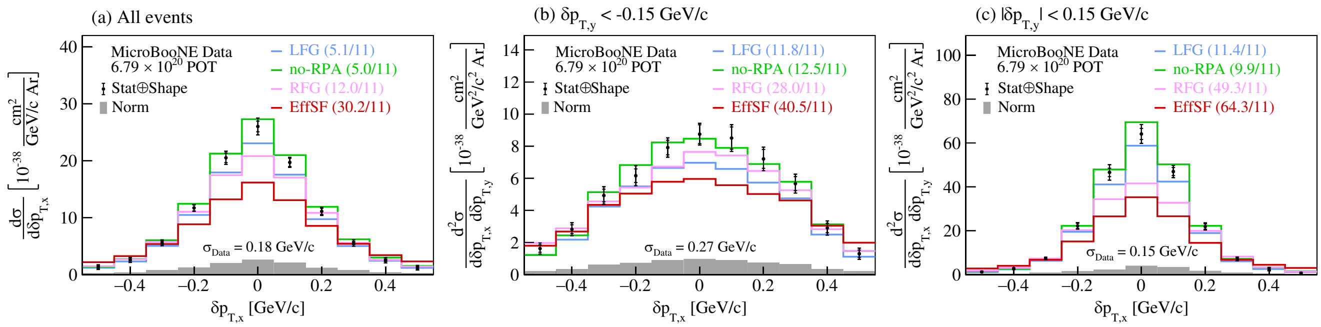

FIG. 3. The flux-integrated (a) single- and (b),(c) double- (in $\delta p_{T,y}$ bins) differential CC1p0π cross sections as a function of the transverse three-momentum transfer component, $\delta p_{T,x}$. Inner and outer error bars show the statistical and total (statistical and shape systematic) uncertainty at the 1σ, or 68%, confidence level. The gray band shows the separate normalization systematic uncertainty. Colored lines show the results of theoretical cross section calculations with a number of event generators. The standard deviation (σ_{Data}) of a Gaussian fit to the data is shown on each panel.

fits on the data distributions. Conversely, the double-differential result for events with $|\delta p_{T,y}| < 0.15$ GeV/c [Fig. 3(c)] shows a much narrower peak which strongly depends on the choice of the underlying model and the inclusion or absence of nuclear effects such as RPA. The LFG and no-RPA predictions are favored in both parts of the phase space. Both the RFG and EffSF predictions illustrate a poor performance in the double-differential measurements and particularly in the QE-dominated $|\delta p_{T,y}| < 0.15$ GeV/c region. The FSI-modeling impact on the same $\delta p_{T,x}$ cross sections is presented in the Supplemental Material [32]. The latter further contains details on the interaction breakdown of various generator predictions for the results reported here, and further single- and double-differential results can be found in Ref. [30].

In summary, we report the first measurement of muon neutrino double-differential cross sections on argon as a function of kinematic imbalance variables for event topologies with a single muon and a single proton detected in the final state. We identify parts of the phase space where the Fermi motion can be largely disentangled from FSI and multinucleon effects. This disentanglement provides leverage to improve separate parts of the complicated neutrino interaction models that affect single-differential distributions in similar ways. Therefore, the reported results pave the path to substantially reducing cross section systematic uncertainties which will enable precision measurements of fundamental neutrino properties.

This document was prepared by the MicroBooNE Collaboration using the resources of the Fermi National Accelerator Laboratory (Fermilab), a U.S. Department of Energy, Office of Science, HEP User Facility. Fermilab is managed by Fermi Research Alliance, LLC (FRA), acting under Contract No. DE-AC02-07CH11359. This material is based upon work supported by Laboratory Directed Research and Development (LDRD) funding from Argonne National Laboratory, provided by the Director, Office of Science, of the U.S. Department of Energy under Contract No. DE-AC02-06CH11357. MicroBooNE is supported by the following: the U.S. Department of Energy, Office of Science, Offices of High Energy Physics and Nuclear Physics; the U.S. National Science Foundation; the Swiss National Science Foundation; the Science and Technology Facilities Council (STFC), part of the United Kingdom Research and Innovation; the Royal Society (United Kingdom); the UK Research and Innovation (UKRI) Future Leaders Fellowship; and the NSF AI Institute for Artificial Intelligence and Fundamental Interactions; and The European Union's Horizon 2020 Marie Sklodowska-Curie Actions. Additional support for the laser calibration system and cosmic ray tagger was provided by the Albert Einstein Center for Fundamental Physics, Bern, Switzerland. We also acknowledge the contributions of technical and scientific staff to the design, construction, and operation of the MicroBooNE detector as well as the contributions of past collaborators to the development of MicroBooNE analyses, without whom this work would not have been possible.

[*]microboone_info@fnal.gov

[1] M. Tanabashi *et al.* (Particle Data Group), Phys. Rev. D **98**, 030001 (2018).
[2] K. Abe *et al.* (T2K Collaboration), Nature (London) **580**, 339 (2020).
[3] M. A. Acero *et al.* (NOvA Collaboration), Phys. Rev. Lett. **123**, 151803 (2019).
[4] B. Abi *et al.* (DUNE Collaboration), arXiv:1807.10334.
[5] B. Abi *et al.* (DUNE Collaboration), arXiv:1807.10327.
[6] B. Abi *et al.* (DUNE Collaboration), arXiv:1807.10340.
[7] M. Antonello *et al.* (MicroBooNE, LAr1-ND, and ICARUS-WA104 Collaborations), arXiv:1503.01520.
[8] F. Tortorici, V. Bellini, and C. Sutera (ICARUS Collaboration), J. Phys. Conf. Ser. **1056**, 012057 (2018).
[9] B. Abi *et al.* (DUNE Collaboration), arXiv:1807.10334.
[10] S. Dolan, U. Mosel, K. Gallmeister, L. Pickering, and S. Bolognesi, Phys. Rev. C **98**, 045502 (2018).

[11] N. Rocco, A. Lovato, and O. Benhar, Phys. Rev. Lett. **116**, 192501 (2016).

[12] N. Rocco, Front. Phys. **8**, 116 (2020).

[13] K. Abe *et al.* (Hyper-Kamiokande Collaboration), arXiv: 1805.04163.

[14] B. Abi *et al.* (DUNE Collaboration), arXiv:2002.03005.

[15] P. Abratenko *et al.* (MicroBooNE Collaboration), Phys. Rev. Lett. **125**, 201803 (2020).

[16] A. Bodek and T. Cai, Eur. Phys. J. C **79**, 293 (2019).

[17] X.-G. Lu, L. Pickering, S. Dolan, G. Barr, D. Coplowe, Y. Uchida, D. Wark, M. O. Wascko, A. Weber, and T. Yuan, Phys. Rev. C **94**, 015503 (2016).

[18] K. Abe *et al.* (T2K Collaboration), Phys. Rev. D **98**, 032003 (2018).

[19] X.-G. Lu *et al.* (MINERvA Collaboration), Phys. Rev. Lett. **121**, 022504 (2018).

[20] T. Cai *et al.* (MINERvA Collaboration), Phys. Rev. D **101**, 092001 (2020).

[21] L. Bathe-Peters, S. Gardiner, and R. Guenette, arXiv: 2201.04664.

[22] R. Acciarri *et al.* (MicroBooNE Collaboration), J. Instrum. **12**, P02017 (2017).

[23] D. Kaleko, J. Instrum. **8**, C09009 (2013).

[24] R. Acciarri *et al.* (MicroBooNE Collaboration), Eur. Phys. J. C **78**, 82 (2018).

[25] Table 289: Muons in liquid argon (Ar), http://pdg.lbl.gov/2012/AtomicNuclearProperties/MUON_ELOSS_TABLES/muonloss_289.pdf (2012).

[26] S. K. H. Bichsel and D. E. Groom, Passage of particles through matter, PDG Chapter 27, Fig. 27.1 http://pdg.lbl.gov/2005/reviews/passagerpp.pdf (2005).

[27] W. Van De Pontseele, Search for electron neutrino anomalies with the MicroBooNE detector, Ph.D. thesis, Oxford University, 2020.

[28] P. Abratenko *et al.* (MicroBooNE Collaboration), Phys. Rev. D **105**, 112004 (2022).

[29] P. Abratenko *et al.* (MicroBooNE Collaboration), J. High Energy Phys. 12 (2021) 153.

[30] P. Abratenko *et al.* (MicroBooNE Collaboration), companion paper, Phys. Rev. D **108**, 053002 (2023).

[31] P. Abratenko *et al.* (MicroBooNE Collaboration), arXiv: 2211.03734.

[32] See Supplemental Material at http://link.aps.org/supplemental/10.1103/PhysRevLett.131.101802 for the data release, the fake data studies, the vertex distribution across the detector and the relevant efficiency, the cross section interaction breakdowns, and alternative modeling comparisons to the reported cross sections, which includes Ref. [33].

[33] C. Llewellyn Smith, Phys. Rep. **3**, 261 (1972).

[34] W. Tang, X. Li, X. Qian, H. Wei, and C. Zhang, J. Instrum. **12**, P10002 (2017).

[35] C. Adams *et al.* (MicroBooNE Collaboration), Eur. Phys. J. C **79**, 673 (2019).

[36] P. Abratenko *et al.* (MicroBooNE Collaboration), Phys. Rev. Lett. **128**, 151801 (2022).

[37] P. Abratenko *et al.* (MicroBooNE Collaboration), Phys. Rev. D **105**, L051102 (2022).

[38] C. Andreopoulos *et al.*, Nucl. Instrum. Methods Phys. Res., Sect. A **614**, 87 (2010).

[39] C. Andreopoulos *et al.*, arXiv:1510.05494.

[40] K. Abe *et al.* (T2K Collaboration), Phys. Rev. D **93**, 112012 (2016).

[41] P. Abratenko *et al.* (MicroBooNE Collaboration), Phys. Rev. D **105**, 072001 (2022).

[42] S. Agostinelli *et al.* (GEANT4 Collaboration), Nucl. Instrum. Methods Phys. Res., Sect. A **506**, 250 (2003).

[43] R. Pordes and E. Snider, Proc. Sci. ICHEP2016 (**2016**) 182.

[44] E. Snider and G. Petrillo, J. Phys. Conf. Ser. **898**, 042057 (2017).

[45] A. A. Aguilar-Arevalo *et al.*, Phys. Rev. D **88**, 032001 (2013).

[46] P. Abratenko *et al.* (MicroBooNE Collaboration), Eur. Phys. J. C **82**, 454 (2022).

[47] J. Calcutt, C. Thorpe, K. Mahn, and L. Fields, J. Instrum. **16**, P08042 (2021).

[48] K. Mahn, A search for muon neutrino and antineutrino disappearance in the Booster Neutrino Beam, Ph.D. thesis, Columbia University, 2009.

[49] R. Carrasco and E. Oset, Nucl. Phys. **A536**, 445 (1992).

[50] J. Nieves, F. Sanchez, I. R. Simo, and M. J. Vicente Vacas, Phys. Rev. D **85**, 113008 (2012).

[51] J. Engel, Phys. Rev. C **57**, 2004 (1998).

[52] J. Nieves, J. E. Amaro, and M. Valverde, Phys. Rev. C **70**, 055503 (2004).

[53] J. Schwehr, D. Cherdack, and R. Gran, arXiv:1601.02038.

[54] J. A. Nowak (MiniBooNE Collaboration), AIP Conf. Proc. **1189**, 243 (2009).

[55] K. Kuzmin, V. Lyubushkin, and V. Naumov, Phys. Part. Nucl. **35**, S133 (2004).

[56] C. Berger and L. M. Sehgal, Phys. Rev. D **76**, 113004 (2007).

[57] K. M. Graczyk and J. T. Sobczyk, Phys. Rev. D **77**, 053001 (2008); **79**, 079903(E) (2009).

[58] C. Berger and L. M. Sehgal, Phys. Rev. D **79**, 053003 (2009).

[59] D. Ashery, I. Navon, G. Azuelos, H. K. Walter, H. J. Pfeiffer, and F. W. Schleputz, Phys. Rev. C **23**, 2173 (1981).

[60] U. Mosel, Phys. Rev. G **46**, 113001 (2019).

[61] T. Leitner, L. Alvarez-Ruso, and U. Mosel, Phys. Rev. C **73**, 065502 (2006).

[62] T. Sjostrand, S. Mrenna, and P. Z. Skands, J. High Energy Phys. 05 (2006) 026.

[63] L. Alvarez-Ruso *et al.* (GENIE Collaboration), Eur. Phys. J. Spec. Top. **230**, 4449 (2021).

[64] S. Dolan, G. D. Megias, and S. Bolognesi, Phys. Rev. D **101**, 033003 (2020).

[65] S. Dytman, Y. Hayato, R. Raboanary, J. T. Sobczyk, J. Tena-Vidal, and N. Vololoniaina, Phys. Rev. D **104**, 053006 (2021).

[66] D. H. Wright and M. H. Kelsey, Nucl. Instrum. Methods Phys. Res., Sect. A **804**, 175 (2015).

[67] A. Bodek and J. L. Ritchie, Phys. Rev. D **23**, 1070 (1981).

[68] A. M. Ankowski and J. T. Sobczyk, Phys. Rev. C **74**, 054316 (2006).